Neutron-diffraction study of icosahedral Al-Cu-Fe single quasicrystals

M. Cornier-Quiquandon and A. Quivy
Centre d'Etudes de Chimie Métallurgique, CNRS 15, rue G. Urbain, F94407 Vitry CEDEX, France

S. Lefebvre and E. Elkaim
Laboratoire pour l'Utilisation du Rayonnement Electromagnétique, Bâtiment 209d, F91405 Orsay CEDEX, France

G. Heger
Laboratoire Léon Brillouin, Laboratoire Commun du Commissariat à l'Energie Atomique et du CNRS, Centre d'Etudes Nucléaires de Saclay, F91191 Gif-sur-Yvette CEDEX, France

A. Katz
Centre de Physique Théorique, Ecole Polytechnique, F91128 Palaiseau CEDEX, France

D. Gratias
Centre d'Etudes de Chimie Métallurgique, CNRS, 15, rue G. Urbain, F94407 Vitry CEDEX, France
(Received 1 February 1991; revised manuscript received 24 April 1991)

This paper reports neutron-diffraction results on a single icosahedral quasicrystal of Al-Cu-Fe. The basic properties of the structure have been extracted using six-dimensional (6D) Patterson analysis from 219 independent orbits of reflections. Described in 6D space, the structure has hyperspace group $F \otimes m35$ and is defined by the three atomic surfaces located at special points with full icosahedral symmetry of the F lattice. These points are the two inequivalent nodes of the underlying primitive lattice plus one of the two inequivalent body centers, the remaining one being empty. The atomic surfaces are embedded in perpendicular space and are well approximated by polyhedra bounded by two-fold planes. These are a large triacontahedron located at the origin, a triacontahedron of the same size truncated along the five-fold directions at the other node, and a small polyhedron bounded by twofold planes at the occupied body center. Although no speculation has been made for distributing the atomic species within these atomic surfaces, the raw reliability factor between experimental and calculated diffraction intensities is already 0.20 with no fitting parameters and the density is found only 2.9% lower than the experimental one. The model presented here can be considered as a zero-order structure to be used for subsequent modeling. The atomic surfaces generate no unacceptably short distances between atoms. Both interatomic distances and coordination numbers of the three first shells are in good agreement with the most recent extended x-ray-absorption fine-structure results. The atomic surfaces are connected together by 3D pieces embedded in the parallel space. They define a partition of the 6D space in hyperprisms, which can be decomposed in direct products of 3D facets located in perpendicular and parallel spaces similar to the oblique cell decomposition of the 3D Penrose tiling. Phasons can propagate along the five-fold and two-fold directions by atomic jumps of 0.1705 and 0.179 nm, respectively.

I. INTRODUCTION

Since the discovery[1] of an icosahedral phase with long-range order in a rapidly quenched Al-Mn alloy called a quasicrystal (a structure with a quasiperiodic diffraction pattern), numerous investigations (see for instance[2–4]) have shown that this kind of structure is also found in other metallic systems as an equilibrium phase. Hence, shortly after the initial discovery, an icosahedral quasicrystal[5] was found as part of the equilibrium phase diagram of the ternary Al-Li-Cu system.

Concomitantly with the experimental work, geometrical models of "ideal" quasiperiodic tilings were proposed for which the diffraction pattern could be exactly calculated.[6–10] The inherent impossibility for ideal quasiperiodic patterns to develop through strictly local growth rules[11] (finite interaction distances) lead to the reasonable idea that real quasicrystals should possess an "universal" disorder (icosahedral glass models; see for instance Ref. 12) that would result in finite peak widths in the diffraction patterns.

This, indeed, was in conformity with existing materials until the discovery[13,14] of an ideal stable icosahedral phase in the Al-Cu-Fe system that changed the situation. Contrary to all previously known phases, the annealed Al-Cu-Fe alloy lead to diffraction peaks comparable to those of good quality ordinary crystals with a width close to the instrumental width of the best high-resolution diffractometers.[15,16]

At about the same time, random-tiling models were studied[17–20] for which the Fourier spectrum shows a countable set of δ functions for three-dimensional quasiperiodic materials, as for the ideal case, plus an additional diffuse scattering in the wings of the peaks.[21] In that

scheme, the icosahedral tiling is stabilized by phason entropy. It suggests that real quasicrystals should be high-temperature equilibrium phases without necessarily being ground states.

The presently available experimental results are inconclusive for determining whether the internal energy or entropy term is predominant at low temperature. On the one hand, recent *in situ* x-ray-diffraction experiments[22] showed abnormal intensity variations as a function of temperature, which could be attributed to a phase transformation from icosahedral to a periodic structure[23] by lowering the temperature. On the other hand, both diffraction studies and high-resolution electron microscopy pictures failed to find thermal phasons in samples annealed at 800 °C. Also, in a recent systematic exploration[16] of the phase diagram (Al, Cu,Fe), a tiny domain of composition close to $Al_{62}Cu_{25.5}Fe_{12.5}$ has been identified where no transformation occurs as a function of temperature.

The aim of this paper is a crystallographic analysis of the icosahedral phase assumed to be a definite ideal structure. This assumption does not contradict the actually available experimental data: no distinguishable diffuse scattering has ever been observed in our annealed samples. This assumption is also legitimate with respect to the thermodynamic behavior of the samples for which annealing at low temperatures (down to 550 °C) does not induce phase transformations[16] that were indeed observed for other compositions.[24] Finally, it remains legitimate with respect to the random-tiling picture for which the ideal icosahedral structure is the configuration where entropy fluctuations are maximized; it is the "most probable" configuration of the random tiling. In that context, a prescription of the definite locations of the atoms has to be understood as a description of the thermodynamically average structure as it is in ordinary high-temperature phase crystals.

There is no attempt here to propose a precise model from the data using refinement techniques. A refinement requires the introduction of a set of adjustable parameters in the ultimate stage of optimizing the diffraction intensities. The problem of choosing parameters that are physically significant is beyond the scope of this paper and will be addressed in a forthcoming paper. We will restrict the discussion only to the structural properties that are directly obtained from the experimental data.

II. EXPERIMENTAL

A. Preparation

An alloy of nominal composition $Al_{63}Cu_{25}Fe_{12}$ was made by levitation melting the pure elements Al(99.99%), Cu(99.9%), and Fe(99.95%) in a high-frequency furnace in an helium atmosphere. After casting in a water-cooled copper crucible, the alloy was remelted and rapidly quenched from 1150 °C by planar flow casting, resulting in brittle flakes approximately 20 μm thick and 5–10 mm wide. The flakes were subsequently annealed during 4 days in an alumina crucible at 860 °C, just below the peritectic transformation. At this temperature, the alloy is partially melted and large single crystals of the icosahedral phase (that can reach millimeter sizes) grow in the liquid. Single quasicrystals are finally mechanically extracted from the matrix.

B. Laue x-ray analysis

A single crystal of 2 mm in size was chosen for both Laue x-ray analysis and neutron diffraction. An example of a Laue back-reflection pattern taken perpendicular to a fivefold axis is shown in Fig. 1 with well-defined reflections that can all be indexed using the same unique icosahedral six-dimensional (6D) index scheme.

Throughout this paper we use the 6D indexing of Cahn, Schechtman, and Gratias.[25] The projections of a

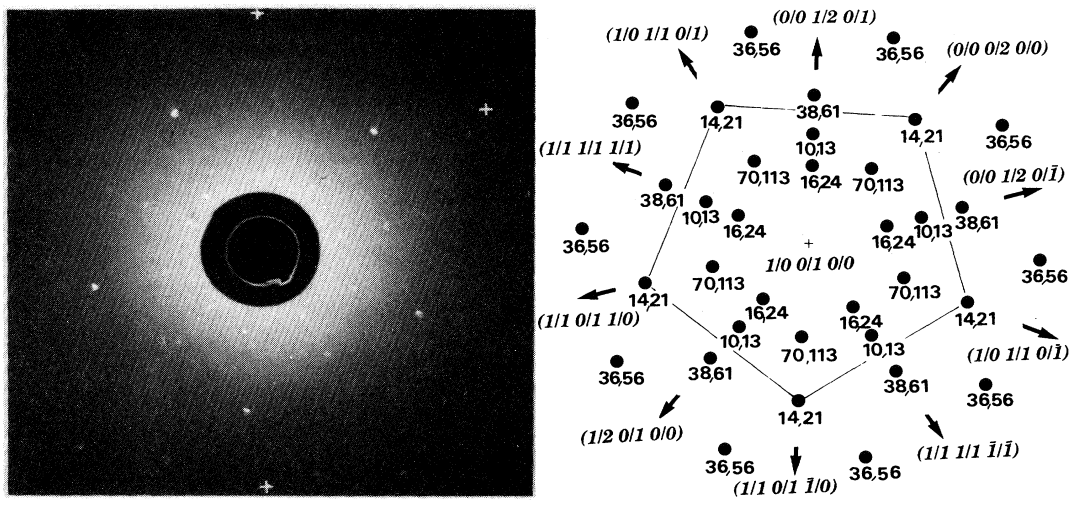

FIG. 1. Backscattering Laue pattern along a five-fold axis (by courtesy of A.M. Waché). Reflections are indexed by doublets N, M according to the indexing scheme of Cahn *et al.* (Ref. 25).

6D reciprocal-lattice vector $\mathbf{Q}=[n_1,n_2,n_3,n_4,n_5,n_6]$ in parallel and perpendicular spaces are given by

$$Q_{x\parallel}=\alpha A^{-1}(h+h'\tau),\quad Q_{y\parallel}=\alpha A^{-1}(k+k'\tau),$$
$$Q_{z\parallel}=\alpha A^{-1}(l+l'\tau),\quad Q_{x\perp}=\alpha A^{-1}(h'-h\tau),$$
$$Q_{y\perp}=\alpha A^{-1}(k'-k\tau),\quad Q_{z\perp}=\alpha A^{-1}(l'-l\tau)$$

with

$$h=n_1-n_4,\quad h'=n_2+n_5,\quad k=n_3-n_6,$$
$$k'=n_1+n_4,\quad l=n_2-n_5,\quad l'=n_3+n_6,$$

where τ is the golden ratio $[\tau=(1+\sqrt{5})/2]$, $\alpha=1/\sqrt{2(2+\tau)}$, and A is the 6D lattice parameter. Two integers N and M, defined by

$$N=h^2+k^2+l^2+h'^2+k'^2+l'^2,$$
$$M=h'^2+k'^2+l'^2+2(hh'+kk'+ll'),$$

are used for labeling the reflections in the powder diffraction patterns. A reflection labeled (N,M) is located in reciprocal space at

$$|Q_\parallel|=\frac{\alpha}{A}\sqrt{N+M\tau},\quad |Q_\perp|=\frac{\alpha}{A}\sqrt{\tau(N\tau-M)}.$$

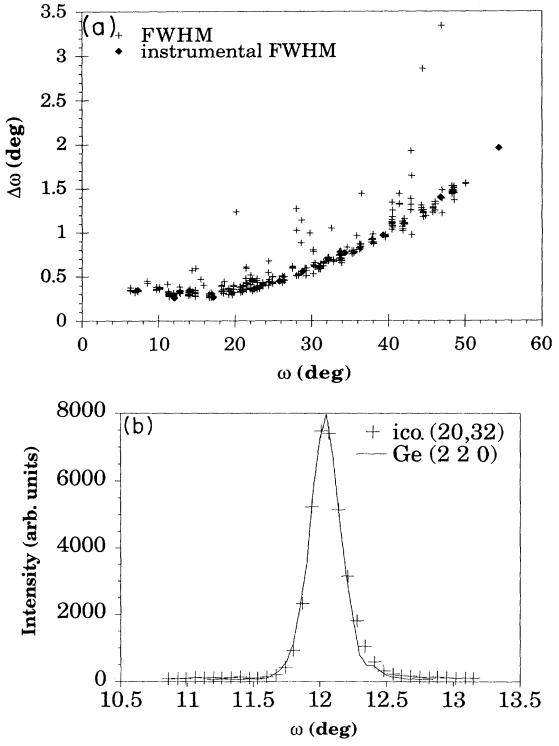

FIG. 2. (a) Full width at half maximum for the icosahedral phase (crosses) as compared to the intrinsic instrumental width obtained from a perfect germanium crystal (full diamonds) as a function of ω angle. All reflections with intensity larger than 10σ correspond to the instrumental width. (b) A typical profile of the intensity of the (20,32) reflection as compared with the (2,2,0) reflection of germanium.

C. Neutron single-crystal diffraction

The neutron measurements were obtained on the four circle diffractometer 5C2 located at the hot source of the Orphée reactor at the Laboratoire Leon Brillouin (LLB) in Saclay (France). The neutron beam is monochromatized by a Cu[111] monochromator at wave length $\lambda=0.8314$ Å.

In five of the 120 elementary sectors of the reciprocal space, 1869 measured integrated intensities were collected by ω scans for θ angles between 5° and 30° and by ω 2θ scans above 30°. From this set, 219 independent orbits have been extracted corresponding to intensities distinguishable from the background.

The 6D primitive lattice parameter, measured from the 25 strongest Bragg reflections, is 0.631 46 nm in agreement with previous measurements.[16] In all cases, the difference between measured and calculated 2θ positions is less than 0.05 degrees.

As shown in Fig. 2(a), the widths of the reflections of intensity higher than 10σ (where σ is the quadratic error) are close to the instrumental width; their profiles are only due to the instrumental divergence as shown in Fig. 2(b) where the (20,32) reflection is superimposed on the [2,2,0] reflection of pure germanium. Reflections between 3σ and 10σ show a systematic deviation consistent with the statistical dispersion expected from low counting rate. The full widths at half maximum (FWHM's) are independent of the perpendicular momentum $Q_\perp$ and of the symmetry of the orbit.

In order to check if equivalent reflections have same intensities, the (20,32) and (18,29) reflections were measured 30 times in three elementary sectors given by the permutation of three of the twofold axes. Whereas the intensities for each reflection are reproducible within 0.05%, the intensities measured in the various sectors vary by 6% or more. The integrated intensity measured as a function of the azimuthal angle Ψ around the scattering vector of the (18,29) reflection oscillates periodically as a function of Ψ (Fig. 3). The amplitude of the oscillation can reach 4.5% of the maximum intensity.

This variation cannot be explained solely by a strong absorption: indeed, the total cross section of the true ab-

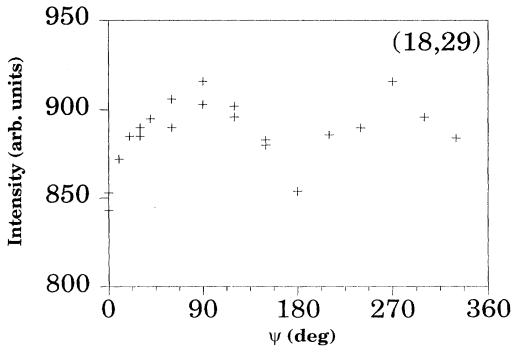

FIG. 3. Integrated intensity for the (18,29) reflection as a function of the azimuthal angle Ψ. Oscillations are observed that could correspond to dynamical diffraction effects.

sorption, the sum of the incoherent and the elastic diffuse cross sections, is reasonably weak ($\mu=0.035$ cm^{-1}) and isotropic (due to the shape of the sample). Moreover, the transmission factor for a sample 2 mm in diameter is 0.993. Dynamical diffraction effects (multiple scattering, secondary extinction) could be responsible for these oscillations, since they are usually magnified in high-quality crystals where spatial correlations extend to large distances. Therefore, a study of the mosaicity of the single crystal has been performed using γ rays from a gold source of 0.03-Å wavelength and 10″ horizontal divergence. Owing to the smallness of the crystal, rocking curves of three (20,32) reflections were measured only for a zero Ψ angle: the FWHM varies from 0.04 to 0.06, values that are only one order of magnitude higher than those obtained with a good silicon crystal (0.008°) and slightly smaller than those obtained from good-quality metallic alloys. Consequently, our sample can be considered as a good-quality metallic alloy in which, indeed, dynamical effects should play an important role enhanced by the unusually high multiplicities of the reflections in reciprocal space.

The external deviation, σ_{ext}, defined as the square root of the mean variance and the internal standard deviation, σ_{int}, defined as the root-mean-square error of equivalent reflections are calculated, respectively, from statistical errors on each integrated intensity and from the dispersion of equivalent measurements (see, for example, Ref. 26). The ratio $\sigma_{\text{int}}/\sigma_{\text{ext}}$, close to one for kinematical diffraction free from anisotropic extinction, provides an estimate of the consistency of the data. Note that the ratio attains high values ($\approx 4-5$) for intense reflections such as (18,29), (20,32), (52,84), and (136,220) where dynamical diffraction effects are expected to be strongest.

III. CRYSTALLOGRAPHIC ANALYSIS

Diffraction experiments give the intensities of the Fourier components of the structure. The determination of the structure by inverse Fourier transform requires solving the phase problem and is not a trivial task.

In the case where a quasicrystalline structure can be obtained from a set of similar chemical species but associated with strongly different scattering form factors, a contrast variation method has been applied for determining the average structures for Al-Mn-Si and Al-Li-Cu using isomorphic and isotopic substitutions in neutron diffraction.[27]

Also, since most of the icosahedral phases like incommensurate structures, are closely related to a "parent" known crystalline phase,[28] an astute technique has been developed by Jaric and Qiu,[29] which consists in reconstructing the missing phases of the quasicrystal through an optimization algorithm from the corresponding phases of the parent crystal.

The case of Al-Cu-Fe does not easily fit into either of these two classes. First, the structure is extremely sensitive to composition, and the preparation of single crystals is not sufficiently well mastered to be safely applied to isotopic substitution of Cu and Fe. Second, no known crystalline phase of the phase diagram has been clearly identified as a rational approximant of the icosahedral structure. We therefore considered the problem in its whole generality of the determination of a 6D periodic object, where atoms are represented by "atomic surfaces" as described by Bak.[30]

A complete crystallographic determination of an ideal quasiperiodic structure (definite structure without disorder) requires several steps, some being equivalent to those encountered in standard crystallography, others being specific to quasicrystallography. They are (i) the determination of the 6D space group of the structure, (ii) the determination of the locations of the atomic surfaces in 6D, (iii) the determination of the geometrical shapes of the atomic surfaces, (iv) the attribution of the chemical species within these atomic surfaces, and (v) a refinement process of these positions in parallel space together with the associated Debye-Waller factor for each of them.

Steps (i), (ii), and (v) are natural extensions of procedures used in standard crystallography, whereas steps (iii) and (iv) are specific to quasicrystals and cannot be numerically handled without considering additional physical assumptions for reducing the (*a priori*) infinite number of fitting parameters to a finite number.[31,32] The present discussion includes steps (i) and (ii) and, to some extent, some basic ideas about the atomic surfaces from step (iii). The remaining steps, requiring the description of specific models, will not be treated here.

All diffraction experiments (x ray, electron, and neutron) clearly show that the 6D lattice is face centered $F(2\,\mathbf{A})$ with no systematic extinctions.[33] Electron microscopy has clearly revealed the presence of antiphase domains but no inversion domains.[34,35] This is in strong support of the centered[36] symmorphic icosahedral group $F\otimes m35$. As it is very convenient to consider an F lattice as a superstructure of order 2 (in any dimension) of a P lattice of parameter A, we shall make the convention throughout this paper of using the underlying primitive lattice as the unit for labeling the sites. Under this convention, the lattice parameter of the F lattice is $2\,\mathbf{A}$ ($A=0.631\,46$ nm).

A. Reciprocal space analysis

The scattering amplitude of an icosahedral quasiperiodic structure can be written as

$$F(\mathbf{Q})=\sum_N \sum_j b_j G_j(\mathbf{Q})\delta(\mathbf{Q}-\mathbf{Q}_N)\ , \tag{1}$$

where j labels the atomic species within the unit cell in 6D space, b_j is the corresponding atomic scattering factor, and $G_j(\mathbf{Q})$ is the Fourier transform of the corresponding atomic surface.

Atomic surfaces are 3D volumes transverse to the parallel space. In all currently known quasicrystals, including Al-Cu-Fe, as will be shown later, Patterson functions show peaks extended along the perpendicular space. Therefore, we make the assumption that the atomic surfaces can be described by a set of elementary volumes (in principle, not necessarily connected) embedded in the perpendicular space. This infinite set of volumes is periodic, i.e., it is generated by a finite number of elemen-

tary volumes located inside the Wigner-Seitz cell of the 6D lattice through the translational symmetry.

We classify these volumes into subsets using the criterion that all volumes belonging to the same subset project *at the same position* $\mathbf{u}_\parallel$ *in parallel space.* Each subset, say S_j, has to be assigned a precise location in 6D space. This location, in principle a matter of convention, can *a priori* be any arbitrary point. Of course, in the most general case, there are no special points in the unit cell to which the atomic surface can be assigned. However, an important remark is that for "simple" structures having a few number of different atomic surfaces, there exist "natural" points for the 6D location of atomic surfaces. The choice is based on symmetry arguments: each subset has an invariant symmetry point group H_{S_j}, a subgroup of the space group, which transforms the elementary volumes of the subset into each other. We define the location $\mathbf{u}_j$ of the subset j in the 6D space as the *invariant point* of H_{S_j}, if it exists and is unique. This definition is not general and applies only if H_{S_j} is a centered group (in this case the invariant set has dimension zero, i.e., it is a single point). In all other cases, an additional decision has to be taken for defining the location within the invariant subspace of H_{S_j}.

The Fourier transform of the atomic surface generated by S_j, say $G_j(\mathbf{Q})$ can be expressed as

$$G_j(\mathbf{Q})=\mu_j e^{2i\pi\mathbf{Q}\cdot\mathbf{u}_j}\int_{S_j} e^{2i\pi\mathbf{Q}_\perp\cdot\mathbf{u}_\perp}d\mathbf{u}_\perp\ , \tag{2}$$

where μ_j is the multiplicity of the $\mathbf{u}_j$ position of the S_j in 6D space and $\mathbf{Q}=\mathbf{Q}_\parallel+\mathbf{Q}_\perp$. The multiplicity μ_j is the index $[m35;H_{S_j}]$ of H_{S_j} in the symmetry-point group of the structure. It is the exact 6D extension of the usual notion of multiplicity encountered in standard crystallography.

Observe that when H_{S_j} is a centered group, the integral in (2) is a real number so that the phases involved in the total diffracted amplitude $G_j(\mathbf{Q})$ are solely due to the exponential factor preceding the integral. This phase is an *intrinsic geometric property* of the 6D lattice and is therefore independent of the actual shapes of the atomic surfaces (up to a sign).

In the special case of neutron diffraction, the atomic form factors are described by the scattering lengths of the nuclei and have constant value in the reciprocal space. Thus, for small $\mathbf{Q}_\perp$ values, the integral (2) converges to the volume V_j of the atomic surfaces so that the total scattering factor $F(\mathbf{Q})$ becomes

$$F(\mathbf{Q})_{\mathbf{Q}_\perp\to 0}=\sum_j \mu_j b_j e^{2i\pi\mathbf{Q}\cdot\mathbf{u}_j}V_j\ . \tag{3}$$

Therefore, if the structure in 6D is simple enough, one could expect that a plot of $|F(\mathbf{Q})|$ as function of $|\mathbf{Q}_\perp|$ will reveal a splitting of the scattered amplitudes into branches, each associated to a possible constant value of the phase $2\pi\mathbf{Q}\cdot\mathbf{u}_j$. Each branch should then have a smooth behavior as a function of $|\mathbf{Q}_\perp|$.

Indeed, in the present experimental data shown in Fig. 4(a), a tendency is observed for a splitting into four

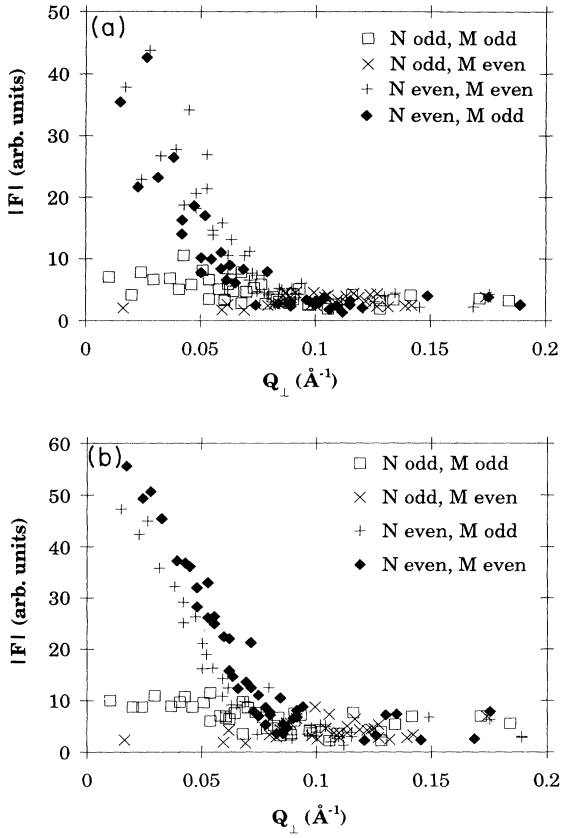

FIG. 4. (a) Raw experimental integrated scattering amplitudes $|F|=\sqrt{I}$ as a function of $|Q_\perp|$. (b) Same plot after Debye-Waller corrections with $B=0.9$ Å^2. A splitting into four branches is now clearly visible at small $|Q_\perp|$.

branches. Now, reflections with comparable perpendicular momenta generally have quite different parallel components, so that a Debye-Waller correction $f_{\mathrm{DW}}=\exp[-(B/4)\mathbf{Q}_\parallel^2]$ of the intensities is of primary importance for revealing the actual splitting.

Assuming that the experimental data should be smooth functions at small $\mathbf{Q}_\perp$, we approximated the intensities in each branch using a fourth-order polynomial with one adjustable Debye-Waller coefficient. We found minimal fluctuations of the experimental data with an average Debye-Waller coefficient $B\sim 0.9$ Å^2, which is a typical value for aluminum at room temperature. Figure 4(b) shows the plot obtained with the corrected amplitudes where the four branches are now clearly visible. At that level of smoothness we were not able to recognize any additional splitting of each branch, the fluctuations being within the accuracy of the intensity measurements. The branches rapidly become intricate for larger $\mathbf{Q}_\perp$ values. They oscillate in a rather complicated way and take values much larger than those expected from spherical atomic surfaces.

This decomposition into only four branches indicates that the locations $\mathbf{u}_j$ of the atomic surfaces are simple ra-

tional points of the 6D lattice. Sorting the branches by descending intensities extrapolated to $\mathbf{Q}_\perp=0$, we observe that the first branch, corresponding to the highest intensities, consists of the reflections with both N and M even, the second branch corresponds to reflections with N even and M odd, the third one to N odd and M odd, and the fourth one to N odd and M even.

It is straightforward arithmetics to show that N and M match the formal group-subgroup decomposition from $I(\mathbf{A})$ to $F(2\mathbf{A})$ according to their parity,

$$I(\mathbf{A}) \longrightarrow P(\mathbf{A}) \longrightarrow F(2\mathbf{A})$$

$$N=4p,\ M=4q \quad + \quad N=2p,\ M=2q+1 \quad + \quad \begin{matrix} N=4p-1,\ M=4q \\ N=4p-1,\ M=4q-1 \end{matrix}$$

with the corresponding coset decomposition,

$$\begin{aligned} I(\mathbf{A})=\{&(Id|[0,0,0,0,0,0])+(Id|[1,0,0,0,0,0]) \\ &+(Id|\tfrac{1}{2}[1,1,1,1,1,1]) \\ &+(Id|\tfrac{1}{2}[1,1,1,1,1,1,-1])\}F(2\mathbf{A}) . \end{aligned}$$

Hence, we directly obtain four locations $\mathbf{u}_j$ for the atomic surfaces in 6D space, i.e., $n_1=[0,0,0,0,0,0]$, $n_2=[1,0,0,0,0,0]$, $bc_1=\frac{1}{2}[1,1,1,1,1,1]$, and $bc_2=\frac{1}{2}[1,1,1,1,1,-1]$ (Ref. 37) that match the observed splitting (as will be confirmed by the Patterson function described in the next section). Interestingly enough, all these locations are special points with little group $m35$ of the $F\otimes m35$ group. Each of the atomic surfaces therefore have the full icosahedral symmetry. In that respect, the structure of Al-Cu-Fe, like all those presently known (Al-Li-Cu and Al-Mn-Si) is also a simple structure where the atomic surfaces are located at high-symmetry special points.[38]

We can now obtain a semiquantitative estimate of the scattering power associated with each of these four sites in 6D by extrapolating the experimental curves to $\mathbf{Q}_\perp=0$. As shown in the previous chapter, the scattering amplitudes derived from n_1, n_2, bc_1, and bc_2 have relative phases, which are simply governed by the indices N and M of the reflection: they are, respectively, $+1$, $(-1)^N$, $(-1)^M$, and $(-1)^{(N+M)}$. Let us label, using (a), (b), (c), and (d) the four branches $a=(N$ even, M even), $b=(N$ even, M odd), $c=(N$ odd, M odd), and $d=(N$ odd, M even). Branch (b) corresponds to a "superstructure" from I to P of branch (a), and branches (c) and (d) correspond to a "superstructure" from P to F of branches (a) and (b). At $\mathbf{Q}_\perp\approx 0$, these branches have the following scattering amplitudes:

$$\text{(a) } F_a=|F_{n_1}+F_{n_2}+F_{\mathrm{bc}_1}+F_{\mathrm{bc}_2}| ,$$

$$\text{(b) } F_b=|F_{n_1}+F_{n_2}-F_{\mathrm{bc}_1}-F_{\mathrm{bc}_2}| ,$$

$$\text{(c) } F_c=|F_{n_1}-F_{n_2}-F_{\mathrm{bc}_1}+F_{\mathrm{bc}_2}| ,$$

$$\text{(d) } F_d=|F_{n_1}-F_{n_2}+F_{\mathrm{bc}_1}-F_{\mathrm{bc}_2}| ,$$

where F_{n_1} denotes the scattering amplitude of the node at the origin, F_{n_2} of the node [1,0,0,0,0,0], F_{bc_1} of the body center $\frac{1}{2}[1,1,1,1,1,1]$ and F_{bc_2} of the body center $\frac{1}{2}[1,1,1,1,1,-1]$, which are positive values at $\mathbf{Q}_\perp\approx 0$. Inverting this set of linear relations using the experimental scattering values, we find an unique set[39] of acceptable equivalent solutions. The total scattering power is distributed according to

$$F_{n_1}\approx 40.25\%,\quad F_{n_2}\approx 51.25\% ,$$

$$F_{\mathrm{bc}_1}\approx 8.5\%,\quad F_{\mathrm{bc}_2}\approx 0\% .$$

Note that the bodycenter bc_2 is empty so that the F unit cell contains only three atomic surfaces each with full icosahedral symmetry centered, respectively, at the node n_1, the node n_2 and the body center bc_1.

Although the present structure can be considered, to some extent, as a superstructure of a primitive structure like Al-Mn-Si,[40–42] it does not result from a simple substitutional chemical ordering of this hypothetical primitive structure. A disordering from F to P would imply the creation of a new atomic surface at the body center bc_2 that is empty here. As a consequence, a transition from F to P would imply the appearance of new atomic positions in the real material and, correlatively, the disappearance of old ones. This could explain why the F structure in Al-Cu-Fe is very robust with respect to heat treatments and does not disorder to P up to the melting point.

B. Patterson analysis

To go further in our study, a 6D Patterson analysis (the Patterson or self-correlation function of an icosahedral structure is the 6D Fourier transform of the diffracted intensities[41,43]) has been performed with the 219 orbits of measured reflections.[44] Figure 5(a) shows a 2D cut of the Patterson function along the twofold plane of the physical space. The main feature of the Patterson function is that it exhibits peaks. The use of a large number of reflections in the calculations reveals that these peaks are very sharp. They correspond to projections of either nodes or body centers of a primitive 6D lattice. This location of the peaks is of course the direct space image of the four branches splitting of the diffraction data.

Depicted in the rational 2D planes corresponding to twofold, threefold, and fivefold axes in 6D [Figs. 5(b), 5(c), and 5(d)], the intense peaks are located, as expected, at the nodes and body centers of the primitive lattice [see Figs. 5(c) and 5(d)]. They extend nicely along the perpendicular space. This indicates that, in the present case, the

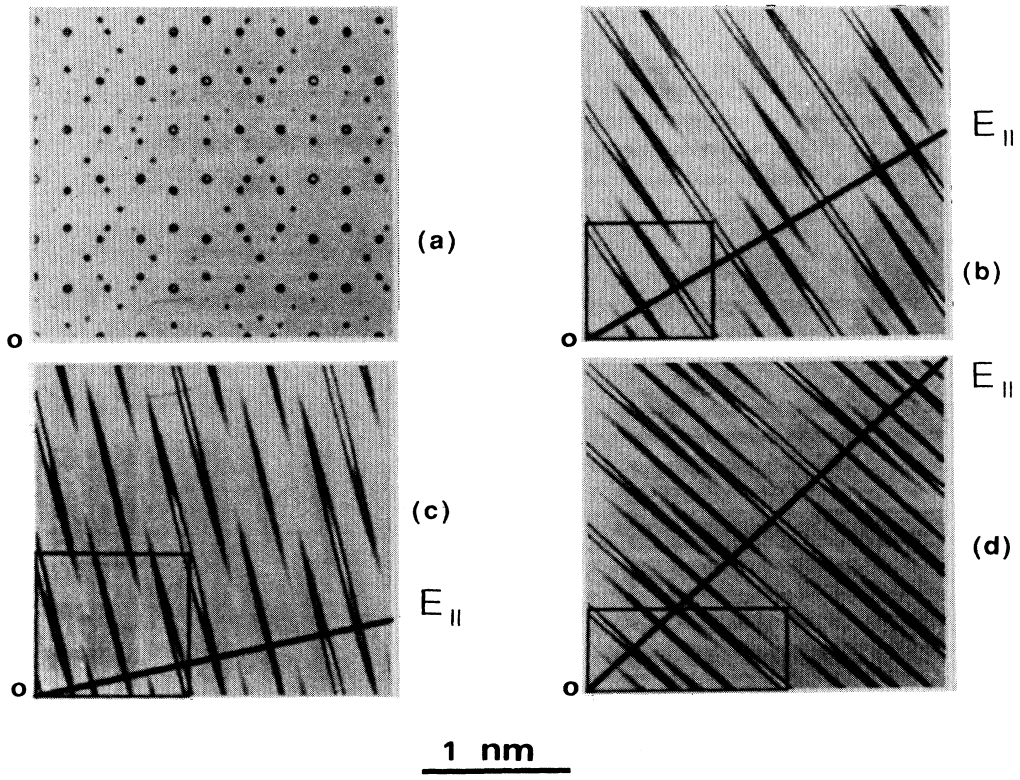

FIG. 5. Patterson contours obtained with 219 orbits of reflections (the contours are visualized by using a pseudogray-scale palette with 10 levels; Patterson functions are normalized between 0 and 255): (a) is a cut in parallel space perpendicular to a 2-fold axis. (b), (c), and (d) are the cut in 6D space along the three basic rational n-fold planes (unit cells are represented by rectangles): (b) two-fold plane $\{[1,1,0,0,0,0],[0,0,1,0,1,0]\}$ passing through the node $[0,0,0,0,0,0]$; (c) threefold plane $\{[1,1,1,0,0,0],[0,0,0,1,1,1]\}$, and (d) fivefold plane $\{[1,0,0,0,0,0],[0,1,1,1,1,-1]\}$.

atomic surfaces are essentially embedded in the perpendicular space with no or little shifting along the parallel space.[45] Our conclusion that the atomic surfaces are (up to the experimental resolution) embedded in 3D planes parallel to the perpendicular space follows from the three following mutually related features of the Patterson function.

(i) In the parallel space, the width of the Patterson peaks corresponds to the minimal width induced by the finite number of components entered into the Fourier synthesis. All peaks are affected the same way irrespective of their locations. If the atomic surfaces were extended along the parallel space, the width of the peaks in the Patterson function would be bounded from below by an intrinsic width (twice larger than this extension) independently of the number of components in the Fourier synthesis.

(ii) The structure of the Patterson function in the neighborhood of the origin (or any F-lattice site) comes only from the superimpositions of the atomic surfaces with themselves. If the atomic surfaces were bent, the amount of superimposition in the neighborhood of the origin would be significantly smaller than at the origin and the Patterson function would exhibit a sharp peak at the origin surrounded by structured wings expanding in both perpendicular and parallel spaces. These features are not observed, clearly implying, together with (i), that *the atomic surfaces are embedded in 3D planes.*

(iii) The structure of the Patterson function in six dimensions is the same in all neighborhoods of nonprimitive translations. This, together with (ii), implies that *the three different atomic surfaces are carried by parallel 3D planes.*

The four peaks in the Patterson function observed in Fig. 5(d) are in agreement with the existence of the three atomic surfaces at n_1, n_2, and bc_1. A rough estimate of the extensions of the peaks at the nodes n_1 and n_2 in the perpendicular space leads to possible atomic surfaces that are scaled by a factor of τ with respect to the canonical triacontahedron associated with the 3D Penrose tilings. Only a careful examination of their relative intensities reveals that the unit cell is $2A$ where the maximum intensity values alternate from odd to even nodes (and body centers) along the [1,0,0,0,0,0] direction. This small difference comes as the image, in direct space, of the relatively low-intensity values of the superstructure reflections (N odd) as compared to the "fundamental" ones (N even).

Plotted in perpendicular space, the Patterson function shows an anisotropy with relatively flat contours along

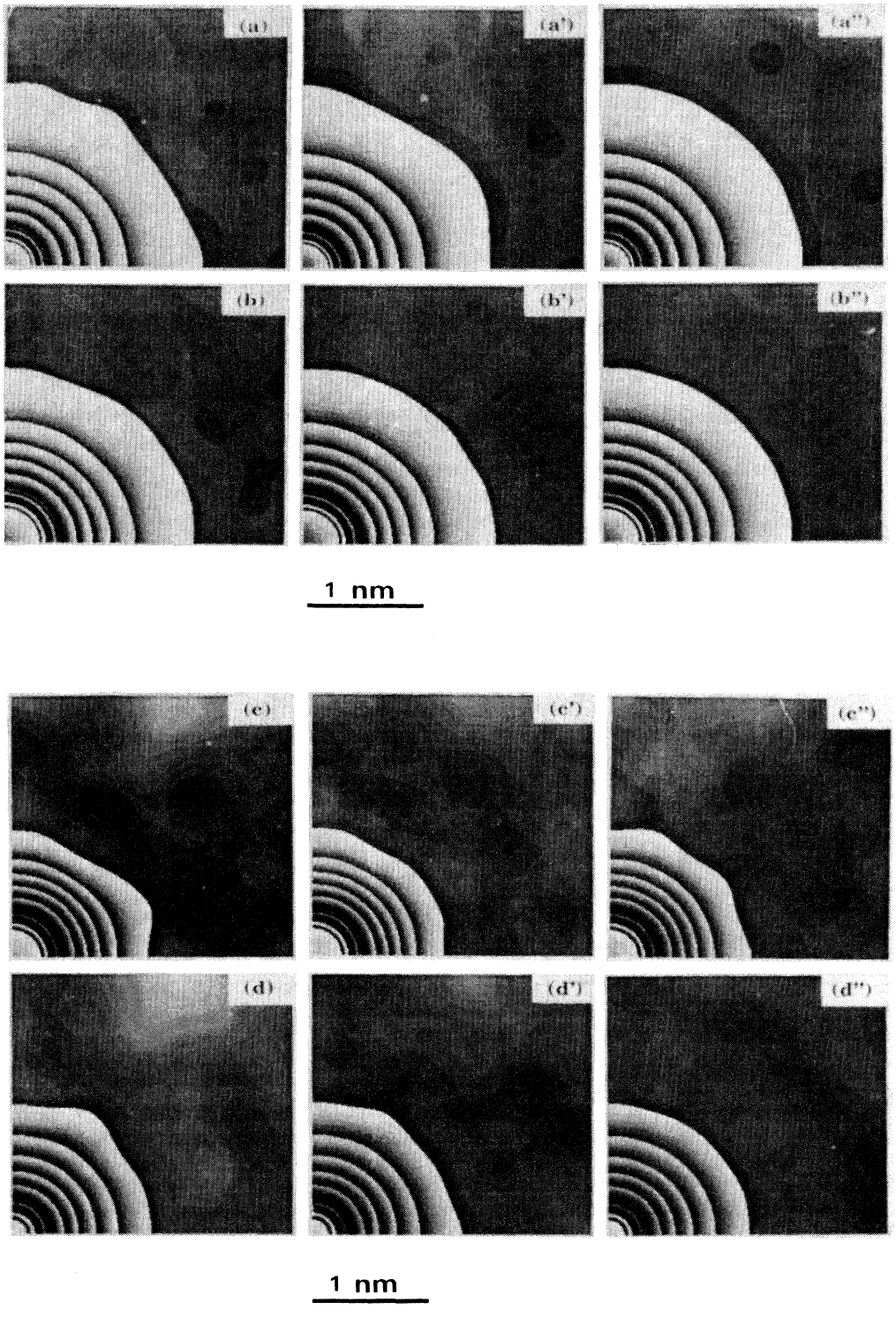

FIG. 6. Patterson cut contours in perpendicular space. The Patterson function decays monotonically from the origin (the visualization of the contours is the same as in Fig. 5). (a,a',a'') at the node n_1 [0,0,0,0,0,0] perpendicular to (a) a twofold axis, (a′) a threefold axis, and (a″) a five-fold axis. (b,b',b'') at the node $n_2=[1,0,0,0,0,0]$ perpendicular to (b) a twofold axis, (b′) a threefold axis, and (b″) a fivefold axis. (c,c',c'') at the body center $bc_1=\frac{1}{2}[1,1,1,1,1,1]$ perpendicular to (c) a twofold axis, (c′) a threefold axis, and (c″) a fivefold axis. (d,d',d'') at the body center $bc_2=\frac{1}{2}[1,1,1,1,1,-1]$ perpendicular to (d) a twofold axis, (d′) a threefold axis, and (d″) a fivefold axis.

the two-fold planes [Figs. 6(a)–6(d)], which suggests that the atomic surfaces are polyhedra bounded by twofold planes. This anisotropy is especially pronounced in the contour maps drawn around the body centers in 6D. The fact is significant considering the high degree of smoothing generated by the self-convolution process.

As shown in Figs. 6(c) and 6(d), interesting features are observed around bc_1 and bc_2. The absence of an atomic surface at the body center bc_2 together with the relatively modest scattering power at the body center bc_1 make the examination of the Patterson function around these two points very interesting. Indeed, what is essentially seen at these points, are the correlations of each of the two major atomic surfaces at the nodes n_1 and n_2 with a small atomic surface located at bc_1, which acts like a probe. The bc_1 translation superimposes the atomic surface of the node n_1 with the one at bc_1 with no contribution of the atomic surface of n_2 and vice versa. The contour shape of the Patterson function at bc_1 is simply related to the shape of the atomic surface of node n_1, whereas at bc_2 it represents the atomic shape located at the node n_2.

The extension of a Patterson map in perpendicular space is roughly given by the sum of the two radii of the overlapping surfaces. A careful examination of the extensions of the Patterson maps leads to the following geometric properties of the atomic surfaces:[46] (i) the polyhedron P_{n_1} at node n_1 is well represented by a triacontahedron of size τ larger than the canonical triacontahedron [Fig. 7(a)], (ii) the polyhedron P_{bc_1} at the body center bc_1 is slightly larger than a triacontahedron of size τ times smaller than the canonical triacontahedron with a maximum diameter along the three-fold axes [Fig. 7(b)], (iii) the polyhedron P_{n_2} at node n_2 is similar to P_{n_1} except that its extension along the fivefold axes is significantly reduced [Fig. 7(c)].

To assign precise shapes for P_{bc_1} and P_{n_2}, we examined the eight basic polyhedra proposed by one of us [A.K. (Ref. 32)] (see the Appendix). Theoretically they come as good candidates for describing atomic surfaces, provided these surfaces are bounded by two-fold planes. One of these polyhedra [Fig. 7(b)] matches the shape and volume requirement for P_{bc_1}.

In order to avoid short distances, we took as P_{n_2}, a large triacontahedron truncated by a $E_\perp$ projection of the fraction in the icosahedral orbit of P_{bc_1} that would generate faulty distances. The intersection occurs around the five-fold axes leading to the truncated triacontahedron seen on Fig. 7(c). This truncation is enough for ensuring that no short distances would come from the atomic surfaces at n_1 and n_2.

Considering now the relative scattering power of each surface, we observe that the strongest scatterer is P_{n_2}, although it is of a smaller size than P_{n_1}. This, of course, is a strong constraint for the chemical ordering of these surfaces. We evaluate the average scattering length $\langle b \rangle$ for each atomic surface ($b_{Al}=0.35$, $b_{Cu}=0.7689$, and $b_{Fe}=0.955$):

$$\langle b_{n_1} \rangle \approx 0.407, \quad \langle b_{bc_1} \rangle \approx 0.775, \quad \langle b_{n_2} \rangle \approx 0.778 .$$

A possibility is that the node n_1 might be mostly occupied by aluminum, the body center by copper, and the node n_2 by a mixture of the three elements (50% Cu, 32% Fe, and 18% Al calculated with the stoichiometry $Al_{63}Cu_{25}Fe_{12}$). In that simple case, the calculated density is 4.28 g/cm^3, i.e., 2.9% below the experimental density.

Diffraction amplitudes have been calculated using these atomic surfaces and the average $\langle b \rangle$ scattering lengths. The results are shown in Fig. 8 as compared to the experimental data. This raw model gives a reliability factor R of 20.6% for 72 reflections which, in our opinion, supports our choice for the atomic surfaces.

This starting value could be minimized by varying the average Debye-Waller factor ($B=0.9$ Å^2) and the three average $\langle b \rangle$'s. At the present stage of the study, such a "cosmetic" fit is not essential for the basic understanding of the structure.

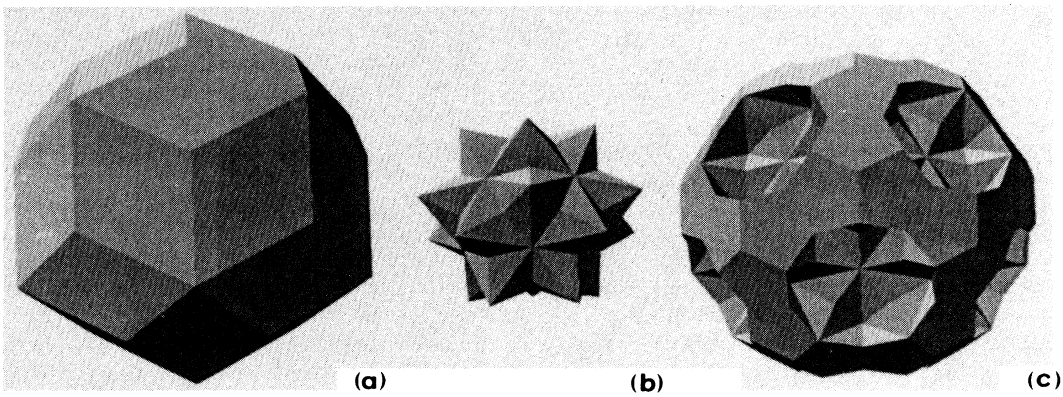

FIG. 7. Atomic surfaces of the model in perpendicular space: (a) P_{n_1} at node n_1 (triacontahedron), (b) P_{bc_1} at body center bc_1, and (c) P_{n_2} at node n_2 (triacontahedron truncated by P_{bc_1}).

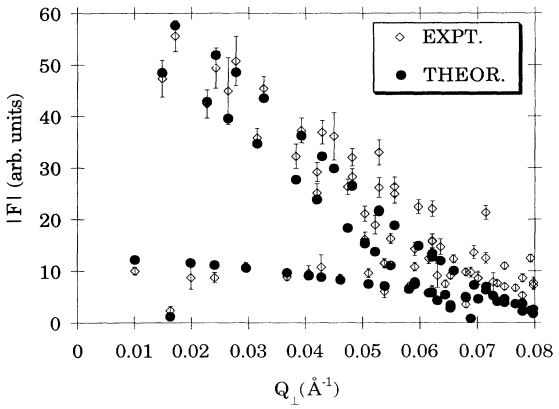

FIG. 8. Theoretical versus experimental scattering amplitudes $|F|$. A reasonable fit is observed for small $\mathbf{Q}_\perp$ values (see text).

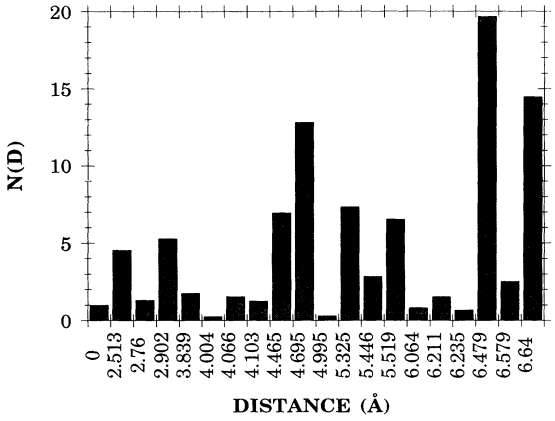

FIG. 9. Coordination numbers $N(d)$ of the first interatomic distances calculated from 3000 atomic sites generated by the model.

C. The quasiperiodic network in icosahedral Al-Cu-Fe

The atomic surfaces P_{n_1} and P_{n_2} both contain the canonical triacontahedron. Therefore, a small fraction of the atomic sites of the structure, irrespective of the chemical species, generates a canonical 3D Penrose tiling by the two basic Ammann rhombohedra with edge $a=0.44648$ nm. However, the locations of the additional atoms cannot be described as a simple atomic "decoration" of these two basic rhombohedra: the presence of the atomic surface at the bodycenter bc_1 and the difference in shape of the atomic surfaces at n_1 and n_2 imply that rhombohedra of the same shape are decorated differently.[47]

The quasiperiodic arrangement of atomic sites must fulfill severe physical constraints. The first requirement is the *absence of inacceptable short distances* and a reasonable distribution of interatomic distances in real space.

To check the atomic framework generated by our set of atomic surfaces, we generated a file of 3000 sites from which we computed the histogram of the coordination numbers for the few first interatomic distances (Fig. 9).

The shortest interatomic distance in the framework is 0.2513 nm with an average coordination number of 4.55. This is a typical Al-Fe or Al-Cu distance in the usual Al_2Cu and Al_3Fe crystals. It is generated by atomic surfaces displaced by a 6D translation of type $\mathbf{t}_1=[1,0,0-1,-1,0]$, which is along a three-fold direction. Since the body center bc_2 is empty, this distance is generated by the pieces of P_{n_1} and P_{n_2} defined by the intersection $P_{n_1}\cap P_{n_2}(\mathbf{t}_1)$ of the $E_\perp$ projections of these two atomic surfaces. Hence, only atom sites derived from either nodes n_1 or n_2 have neighbors at 0.251 nm, located on the vertices of a regular dodecahedron. Their maximum number is 7, and they are never close neighbors to each other.[48]

The second interatomic distance is 0.276 nm with an average coordination number of 1.31. It is generated by atomic surfaces displaced by a 6D translation of type $\mathbf{t}_2=\frac{1}{2}[1,1,1,1,1,1]$, which is along a five-fold direction. This distance arises from the atomic surfaces on nodes n_1 and bc_1 defined by the intersection $P_{n_1}\cap P_{\mathrm{bc}_1}(\mathbf{t}_2)$. Therefore, only atom sites derived from either n_1 and bc_1 have neighbors at 0.276 nm located on the vertices of a regular icosahedron. Since this intersection has a small volume, the average coordination number is low (1.31).

The next interatomic distance, 0.290 nm, has a high coordination number of 5.28 and is typical of Al-Al distances. It comes from both n_1 and n_2 by a translation $\mathbf{t}_3=[0,-1,1,0,1,1]$ along twofold axes and does not arise for atom sites derived from the atomic surfaces located at bc_1. The neighbors are located on the vertices of an icosidodecahedron.

All together these three first distances form the first coordination shell with an average distance of 0.2724 nm and coordination number 11.14.

It is interesting to compare our results with those recently obtained by Sadoc[49] in an EXAFS study of $Al_{65}Cu_{20}Fe_{15}$ and $Al_{63}Cu_{25}Fe_{12}$. First, the distances of interest as revealed by extended x-ray-absorption fine structure (EXAFS) do correspond to ours with an accuracy better than 0.005 nm. Second, the average coordination number for the three first distances are, respectively, 4.6, 2.0, and 4.1 by EXAFS as compared to 4.55, 1.31, and 5.28 in this study.

A second important physical requirement of a quasiperiodic structure is the *closeness property of the atomic surfaces in the 6D torus* (the set of the atomic surfaces should form a manifold without boundaries). This condition ensures that there will be no "annihilation creation" of arbitrarily distant atoms under a translation in perpendicular space.

Indeed, as illustrated on Fig. 10 showing the cuts in 6D space of our atomic surfaces drawn in the twofold-, threefold-, and fivefold 2D axes, the atomic surfaces are connected to each other by 3D polyhedra embedded in parallel space. The facets of the polyhedra are mapped on each other by short translations belonging to the $E_\perp$

projection of the 6D lattice. This generates a partition of R^6 in hyperprisms decomposable into direct products of 3D volumes in $E_\parallel$ and $E_\perp$. This decomposition is similar to the oblique cell decomposition[50–53] previously introduced to partition the 6D space in the standard 3D Penrose tiling.

Our set of atomic surfaces, completed by 3D pieces parallel to the parallel space, form a closed set by construction. As a consequence, phason propagation proceeds only by close-neighbor atomic jumps. The probability of these atomic jumps are given by the overlapping area of the two considered atomic surfaces projected in perpendicular space. As shown on Fig. 10, the shortest jump distance is 0.105 nm along the fivefold axes and connects P_{n_1} to P_{n_2} translated by [1,1,−2,1,−1,1] (and equivalent sites). In our model, this atomic jump should not appear, since these two polyhedra, projected in perpendicular space, connect only by vertices. The second distance is 0.155 nm along the threefold axes. It corresponds to the connection of P_{bc_1} with P_{n_2} translated by $\frac{1}{2}[-3,1,1,3,3,1]$. Here, again, the connection occurs only by vertices and this atomic jump is very unlikely to occur. The next possible atomic jump is 0.1705 nm along the five-fold axes corresponding to the connection of P_{n_2} with P_{bc_1} translated by $\frac{1}{2}[-1,-1,3,-1,1,-1]$. Here the connection occurs by facets (actually *all* facets of P_{bc_1} are concerned). As a result, this atomic jump along five-fold directions should occur very frequently. The last possible atomic jump is 0.179 nm along twofold axes coming from connections between P_{n1} (P_{n2}) with P_{n1} (P_{n2}) translated by [0,2,−1,0,−2,−1]. Here too, the overlapping areas are the facets of the polyhedra, and we expect this atomic jump also to occur frequently in the material.[54]

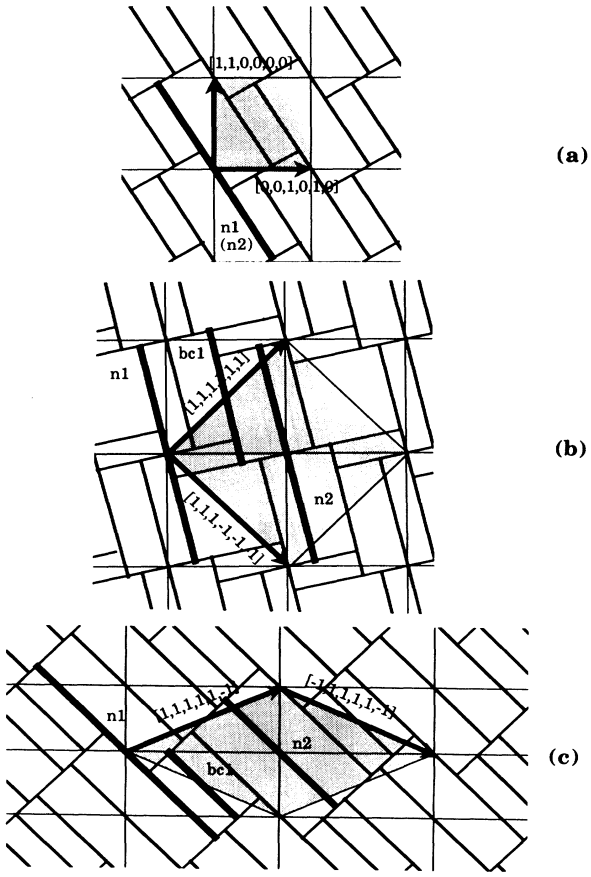

FIG. 10. 2D cuts of the atomic surfaces of the model in 6D showing the decomposition of R^6 in hyperprisms; the thick lines represent the basic atomic surfaces, the thin lines represent the primitive lattice: (a) two-fold plane, (b) three-fold plane, and (c) fivefold plane.

From this simple geometric analysis of our model, we conclude that phason defects in Al-Cu-Fe should have the following characteristics.

(i) Since the atomic surfaces in perpendicular space are faceted by twofold planes, the defects should appear as boundaries oriented along twofold planes in the physical space.

(ii) The atomic jumps are of two kinds: 0.1705 nm along fivefold directions and 0.179 nm along twofold directions.

By electron microscopy, we should observe planar boundaries in the twofold planes and streaks around the diffraction peaks along fivefold directions and/or twofold directions essentially governed by the perpendicular components of the wave vectors (Bessiere *et al.*[55]).

IV. CONCLUSIONS

This study has shown that, as in all known quasicrystalline icosahedral structures, the icosahedral Al-Cu-Fe phase has a simple description in 6D space. The 6D unit cell is face centered and contains three atomic surfaces P_{n1}, P_{n2}, and $P_{\mathrm{bc}1}$, each with full icosahedral symmetry, located, respectively, at the nodes n_1 and n_2 and at the body center bc_1. The body center bc_2 is empty.

The Patterson function analysis has shown that the atomic surfaces are embedded in perpendicular space and are faceted along twofold planes. These planes are privileged planes for easy phason relaxations, since they are the 3D analogs of the worms of zero flipping energy in the 2D Penrose tiling.

Our choice of atomic surfaces guarantees that no unacceptable short distances are generated and that phasons propagate through close-neighbor atomic jumps. Therefore, they should relax easily as indicated by the observed spectacular rapid enhancement of the quality of the icosahedral phase through short time annealing treatments.

No attempt has been proposed here to refine our model. A precise prescription of the atomic species within the atomic surfaces requires further experimental and theoretical studies, which are in progress and will be discussed in subsequent papers.

ACKNOWLEDGMENTS

We very gratefully acknowledge our colleagues Suzanne Peynot, Alain Dezellus, and Patrick Ochin for

the preparation of the master alloy used in this study. We are very pleased to warmly thank Leonid Levitov, Yvonne Calvayrac, Peter Bancel, and Bert Mozer for their many suggestions and criticisms of the results and the manuscript. Finally, special thanks are due to Pierre Bastie for his contribution in the diffraction study of the crystal with γ rays.

APPENDIX: ATOMIC SURFACE POLYHEDRA

The atomic surfaces represent the atomic trajectories under translation in perpendicular space. They must fulfill severe constraints especially the following:[56]

(i) There should be no "annihilation-creation" of arbitrary distant atoms under a translation in perpendicular

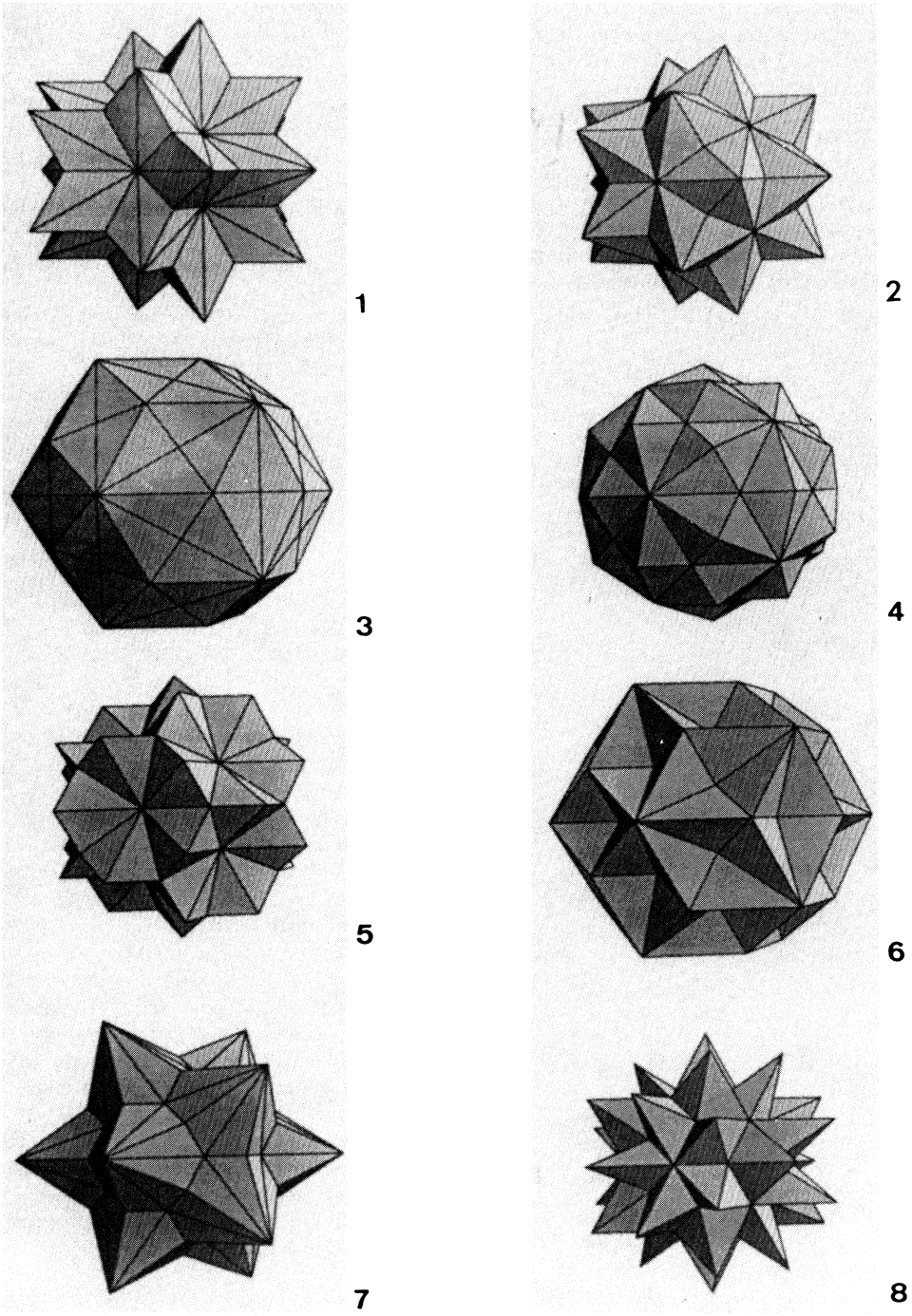

FIG. 11. The eight polyhedra with full icosahedral symmetry constructed with twofold planes as defined in Table I.

TABLE I. The basic polyhedra are defined in the elementary sector by their intersection lengths along the three high symmetry vectors $\mathbf{A}_5=[1,0,\tau]$, $\mathbf{A}_2=[0,0,2\tau]$, and $\mathbf{A}_3=[0,-\tau,\tau^3]$. For example, polyhedron No. 1 is defined by the triangle formed by the extremities of $(\mathbf{A}_5, \mathbf{A}_2, \mathbf{A}_3)$, polyhedron No. 2 by $(\mathbf{A}_5, \tau^{-1}\mathbf{A}_2, \tau^{-1}\mathbf{A}_3)$, etc. The full polyhedron is obtained by applying the 120 operators of $m35$ on the elementary triangle. The scale used in the table is such that the canonical triacontahedron (convex envelope of the projection of the 6D cube in perpendicular space) is polyhedron No. 3 inflated by τ: $(\tau\mathbf{A}_5, (\tau/2)\mathbf{A}_2, \tau^{-1}\mathbf{A}_3)$.

Polyhedron No.	A_5	A_2	A_3
1	1	1	1
2	1	τ^{-1}	τ^{-1}
3	1	$\frac{1}{2}$	τ^{-2}
4	1	τ^{-1}	τ^{-2}
5	1	1	τ^{-1}
6	1	τ^{-2}	τ^{-2}
7	1	τ^{-2}	τ^{-3}
8	1	1	τ^{-2}

space (closeness condition).

(ii) No two atoms should come infinitely close to each other (hard-core condition, nonintersecting atomic surfaces).

In addition to these basic topological constraints, we request the quasiperiodic order to propagate through local rules. A necessary (but not sufficient) condition is that the atomic surfaces be bounded by rational planes of the 6D lattice (polyhedra). In order to achieve the closeness condition, opposite facets of the polyhedra must be mapped on each other by translations belonging to the perpendicular projection of the 6D lattice. Finally we want the atomic jumps to occur in a symmetric environment such that initial and final states have the closest possible configurational energies. These conditions lead to the twofold planes as being the best candidates for possible facets of the polyhedra. It is easily shown (Katz[32]) that only eight basic polyhedra with full icosahedral symmetry can be built from the 15 twofold planes. These polyhedra are listed in Table I and shown on Fig. 11. They can be linearly scaled by any power of τ.

Polyhedron P_{n1} in the text corresponds to polyhedron No. 3 (triacontahedron) inflated by a factor of τ^2 in length, polyhedron P_{bc_1} corresponds to polyhedron No. 2. Polyhedron P_{n2} is obtained by truncating P_{n1} with P_{bc_1} displaced along the perpendicular component (fivefold axis) of the 6D translation $\frac{1}{2}[-1,-1,3,-1,1,-1]$ and its equivalents.

[1]D. Shechtman, I. Blech, D. Gratias, and J. W. Cahn, Phys. Rev. Lett. **53**, 1951 (1984).

[2]*The Physics of Quasicrystals,* edited by P. J. Steinhardt and S. Ostlund (World Scientific, Singapore, 1987).

[3]*Introduction to Quasicrystals,* edited by M. Jaric (Academic, San Diego, 1988).

[4]*QuasiCrystalline Materials,* edited by C. Janot and J.-M. Dubois (World Scientific, Singapore, 1988).

[5]B. Dubost, J.-M. Lang, M. Tanaka, P. Sainfort, and M. Audier, Nature (London) **324**, 48-50 (1986).

[6]D. Levine and P. J. Steinhardt, Phys. Rev. Lett. **53**, 2477 (1984).

[7]M. Duneau and A. Katz, Phys. Rev. Lett. **54**, 2688 (1985).

[8]P. A. Kalugin, A. Y. Kitayev, and L. S. Levitov, J. Phys. (Paris) Lett. **46**, L601 (1985).

[9]V. Elser, Phys. Rev. B **32**, 4892 (1985).

[10]M. Jaric, Phys. Rev. B **34**, 4685 (1986).

[11]R. Penrose, in *Introduction to the Mathematics of Quasicrystals,* edited by M. V. Jaric (Academic, New York, 1989), p. 53–79.

[12]P. M. Horn, W. Malzfeldt, D. P. DiVincenzo, J. Toner, and R. Gambino, Phys. Rev. Lett. **57**, 1444 (1986).

[13]A. P. Tsai, A. Inoue, and T. Masumoto, J. Mater. Sci. Lett. **6**, 1403 (1987).

[14]A. P. Tsai, A. Inoue, and T. Masumoto, Mater. Trans. **30**, 300 (1989).

[15]C. A. Guryan, A. I. Goldman, P. W. Stephens, K. Hiraga, A. P. Tsai, A. Inoue and T. Masumoto, Phys. Rev. Lett. **62**, 2409 (1989).

[16]Y. Calvayrac, A. Quivy, M. Bessiere, S. Lefebvre, M. Cornier-Quiquandon, and D. Gratias, J. Phys. (Paris) **51**, 417 (1990).

[17]M. Jaric and U. Mohanty, Phys. Rev. Lett. **58**, 230 (1987).

[18]K. J. Strandburg, L. H. Tang, and M. V. Jaric, Phys. Rev. Lett. **63**, 314 (1989).

[19]M. Widom, D. P. Deng, and C. L. Henley, Phys. Rev. Lett. **63**, 310 (1989).

[20]C. L. Henley, in *Third International Meeting on Quasicrytals; Quasicrystals and Incommensurate Structures* (World Scientific, Vista Hermosa, Mexico, 1989), pp. 152–169.

[21]L.-H. Tang, Phys. Rev. Lett. **64**, 2390 (1990).

[22]P. A. Bancel, Phys. Rev. Lett. **63**, 2741 (1989).

[23]M. Audier and P. Guyot, in *Third International Meeting on Quasicrystals* (World Scientific, Vista Hermosa, Mexico, 1990), p. 288–299.

[24]M. Audier and P. Guyot, in *Proceedings of the Anniversary Adriatico Research Conference* on Quasicrystals (World Scientific, Trieste, Italy, 1990), pp. 74–91.

[25]J. W. Cahn, D. Schechtman, and D. Gratias, J. Mater. Res. **1**, 13 (1986).

[26]R. Blessing, Crystallogr. Rev. **1**, 3 (1987).

[27]M. deBoissieu, C. Janot, J.-M. Dubois M. Audier, and B. Dubost, J. Phys. (Paris) **50**, 1689 (1989).

[28]V. Elser and C. L. Henley, Phys. Rev. Lett. **55**, 2883 (1985).

[29]M. V. Jaric and S.-Y. Qiu, in *(Quasicrystals 12th Taniguchi Symposium)* (Springer-Verlag, Shima, Japan, 1990), pp. 48–56.

[30]P. Bak, Scr. Metall. **20**, 1199 (1986).

[31]P. Bak, Phys. Rev. Lett. **56**, 861 (1986).

[32]A. Katz, in *Number Theory and Physics,* edited by J.-M. Luck, P. Moussa, M. Waldschmidt, and C. Itzykson (Springer-Verlag, Berlin, in press).

[33]The 6D lattices consistent with icosahedral symmetry are grouped into three classes: the body center $I(\mathbf{A})$ lattice

formed by the set of integers and half integers $\{[n_1,n_2,n_3,n_4,n_5,n_6], [n_1+\frac{1}{2}, n_2+\frac{1}{2}, n_3+\frac{1}{2}, n_4+\frac{1}{2}, n_5+\frac{1}{2}, n_6+\frac{1}{2}]\}$, the primitive $P(\mathbf{A})$ lattice formed by the set of integers $\{[n_1,n_2,n_3,n_4,n_5,n_6]\}$, and the face centered $F(2\mathbf{A})$ lattice formed by the set of integers with even sum. They are related group-subgroups $I(\mathbf{A}) > P(\mathbf{A}) > F(2\mathbf{A})$, with index 2 between two successive groups. A is the 6D lattice parameter.

[34]S. Ebalard and F. Spaepen, J. Mater. Res. **4**, 39 (1989).

[35]J. Devaud-Rzepski, A. Quivy, Y. Calvayrac, M. Cornier-Quiquandon, and D. Gratias, Philos. Mag. B **60**, 855 (1989).

[36]Although the noncentered group $F\otimes 235$ cannot be absolutely ruled out, a careful examination of multibeam diffraction contrast in electron microscopy using polar reflections of 235 always revealed identical contrasts between variants as expected from a centered structure.

[37]Observe that, contrary to fcc $Fm3m$ in 3D where the positions $[\frac{1}{4},\frac{1}{4},\frac{1}{4}]$ and $[\frac{1}{4},\frac{1}{4},\frac{3}{4}]$ belong to the same orbit, these two body centers in 6D define two different orbits.

[38]This intriguing fact brings up an interesting question. Could any additional simplification be achieved using a space with dimension larger than 6 (maybe a 10 D space) where these atomic surfaces would group into a single one? Let us recall that the perfect Penrose tiling can be equivalently generated either from a 4D space using five atomic surfaces located at special points of the 4D lattice, or from a 5D space with an unique atomic volume.

[39]There are, of course, four equivalent settings depending on where the origin is chosen.

[40]J. W. Cahn, D. Gratias, and B. Mozer, J. Phys. (Paris) **49**, 1225 (1988).

[41]J. W. Cahn, D. Gratias, and B. Mozer, Phys. Rev. B **38**, 1638 (1988).

[42]M. Duneau and and C. Oguey, J. Phys. (Paris) **50**, 135 (1989).

[43]D. Gratias, J. W. Cahn, and B. Mozer, Phys. Rev. B **38**, 1643 (1988).

[44]A list of the experimental diffraction intensities is available on request to the authors.

[45]Observe that the Patterson function of a general quasiperiodic discrete structure is not necessarily discrete, i.e., does not necessarily exhibits sharp peaks in parallel space.

[46]In that case, the extensions along the various axes are expected to be close to $(\tau^2+1)\,\mathbf{e}_j$, where the $\mathbf{e}_j$ are the basic vectors of the triacontrahedron τ times smaller than the canonical one along the twofold, threefold and fivefold axes given by

$$e_2=\frac{\tau A}{\sqrt{2(2+\tau)}},\quad e_3=\frac{\sqrt{3}A}{\sqrt{2(2+\tau)}},\quad e_5=\frac{A}{\sqrt{2}},$$

where A designates the lattice parameter in 6D (here, $A=0.62$ nm, $e_2=0.38$ nm, $e_3=0.41$ nm, and $e_5=0.45$ nm).

[47]Observe that this does not forbid the structure to have local rules.

[48]Such a configuration would generate an unacceptable interatomic distance of 0.17 nm.

[49]A. Sadoc (private communication).

[50]C. Oguey, M. Duneau, and A. Katz, Commun. Math. Phys. **118**, 99 (1988).

[51]P, Kramer, J. Math. Phys. **29**, 516 (1988).

[52]A. Katz, in *Introduction to the Mathematics of Quasicrystals*, edited by M. V. Jaric (Academic, New York, 1989), pp. 53–79.

[53]V. I. Arnol'd, Physica D **33**, 21 (1988).

[54]The four distances for the possible atomic jumps are robust values. They are coming directly from 6D geometry. Other sets of atomic surfaces at the nodes and one body center, that would be consistent with density and diffraction data, would lead to the same possible atomic jump distances. Only the jump frequencies may change according to the type of connections between the chosen polyhedra.

[55]M. Bessiere *et al.* (unpublished).

[56]D. M. Frenkel, C. L. Henley, and E. D. Siggia, Phys. Rev. B **34**, 3649 (1986).

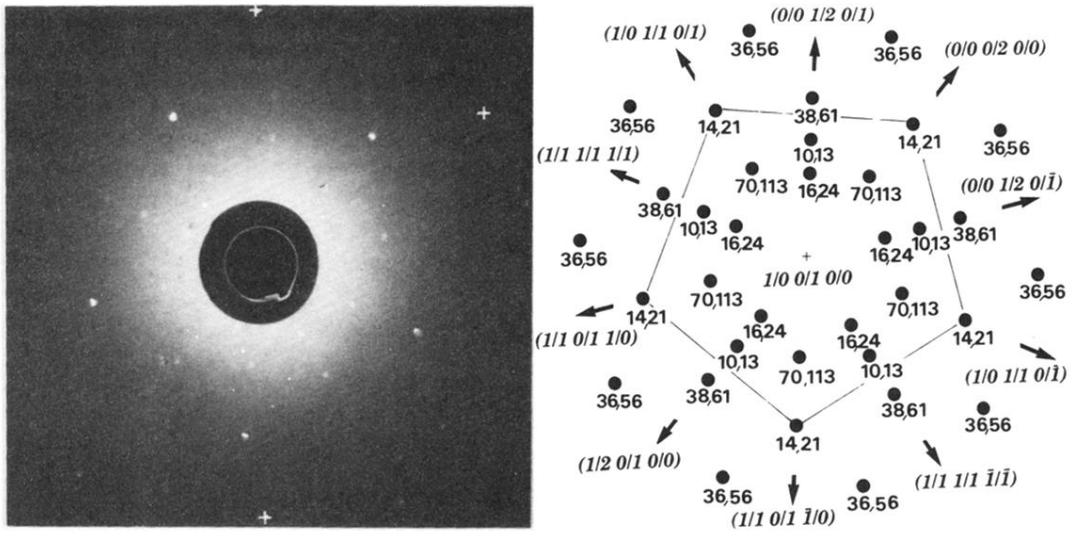

FIG. 1. Backscattering Laue pattern along a five-fold axis (by courtesy of A.M. Waché). Reflections are indexed by doublets N,M according to the indexing scheme of Cahn *et al.* (Ref. 25).

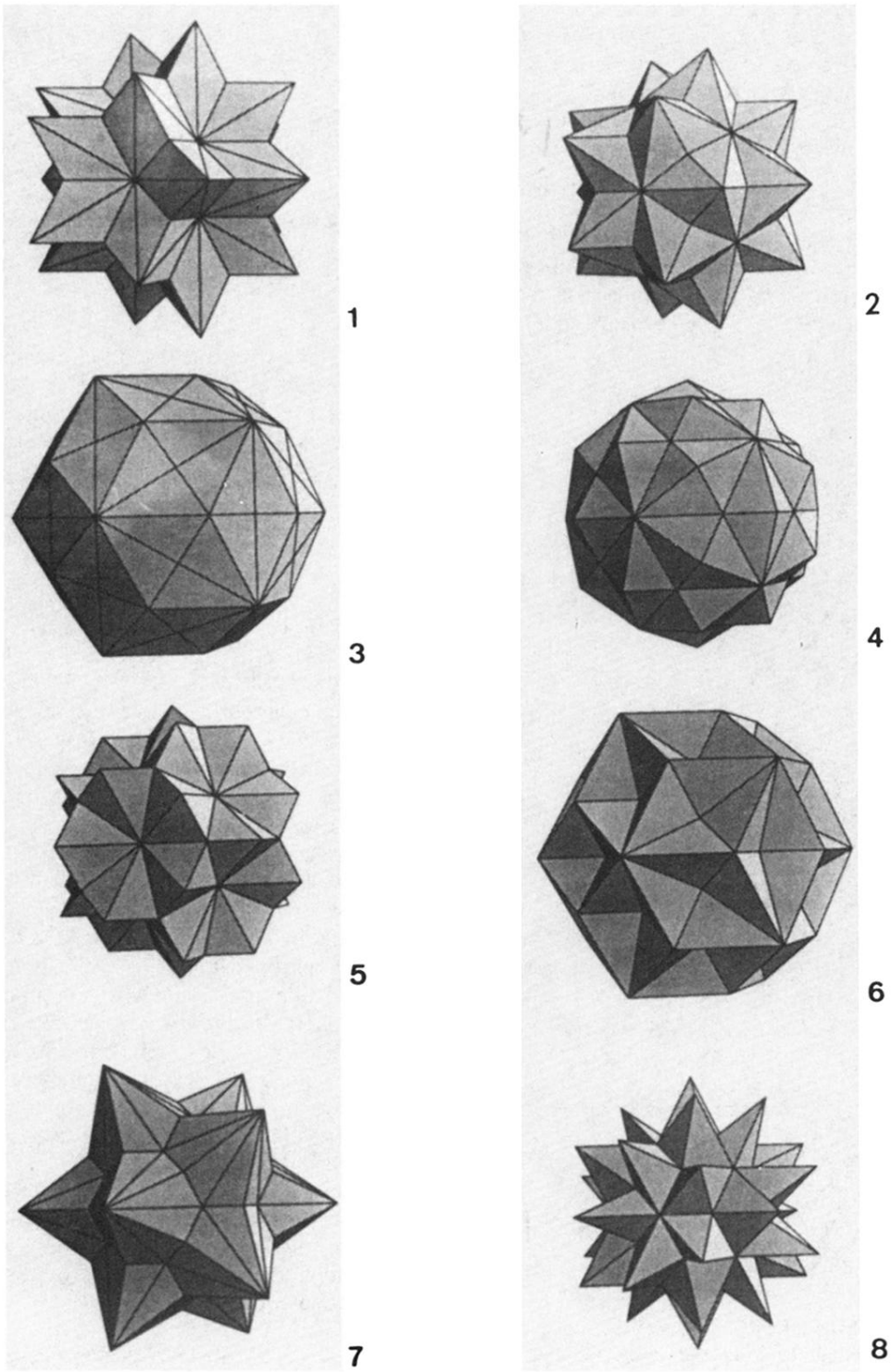

FIG. 11. The eight polyhedra with full icosahedral symmetry constructed with twofold planes as defined in Table I.

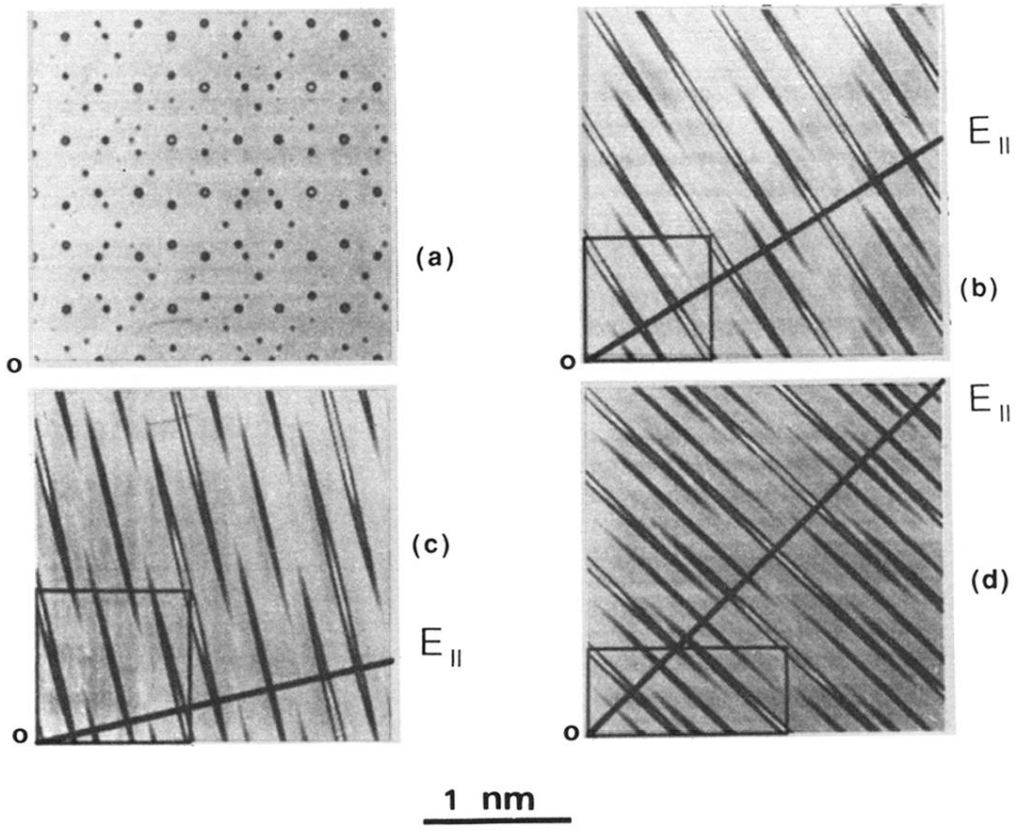

FIG. 5. Patterson contours obtained with 219 orbits of reflections (the contours are visualized by using a pseudogray-scale palette with 10 levels; Patterson functions are normalized between 0 and 255): (a) is a cut in parallel space perpendicular to a 2-fold axis. (b), (c), and (d) are the cut in 6D space along the three basic rational n-fold planes (unit cells are represented by rectangles): (b) two-fold plane $\{[1,1,0,0,0,0], [0,0,1,0,1,0]\}$ passing through the node $[0,0,0,0,0,0]$; (c) threefold plane $\{[1,1,1,0,0,0],[0,0,0,1,1,1]\}$, and (d) fivefold plane $\{[1,0,0,0,0,0],[0,1,1,1,1,-1]\}$.

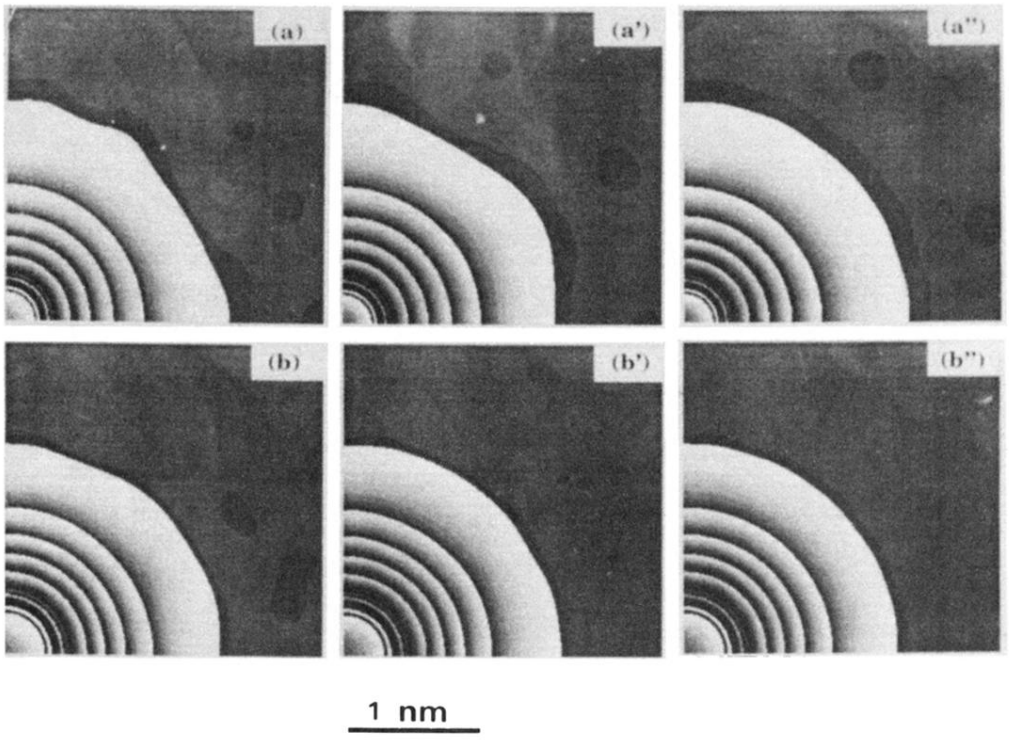

FIG. 6. Patterson cut contours in perpendicular space. The Patterson function decays monotonically from the origin (the visualization of the contours is the same as in Fig. 5). (a,a',a'') at the node n_1 [0,0,0,0,0,0] perpendicular to (a) a twofold axis, (a′) a threefold axis, and (a″) a five-fold axis. (b,b',b'') at the node $n_2=[1,0,0,0,0,0]$ perpendicular to (b) a twofold axis, (b′) a threefold axis, and (b″) a fivefold axis. (c,c',c'') at the body center $\mathrm{bc}_1=\frac{1}{2}[1,1,1,1,1,1]$ perpendicular to (c) a twofold axis, (c′) a threefold axis, and (c″) a fivefold axis. (d,d',d'') at the body center $\mathrm{bc}_2=\frac{1}{2}[1,1,1,1,1,-1]$ perpendicular to (d) a twofold axis, (d′) a threefold axis, and (d″) a fivefold axis.

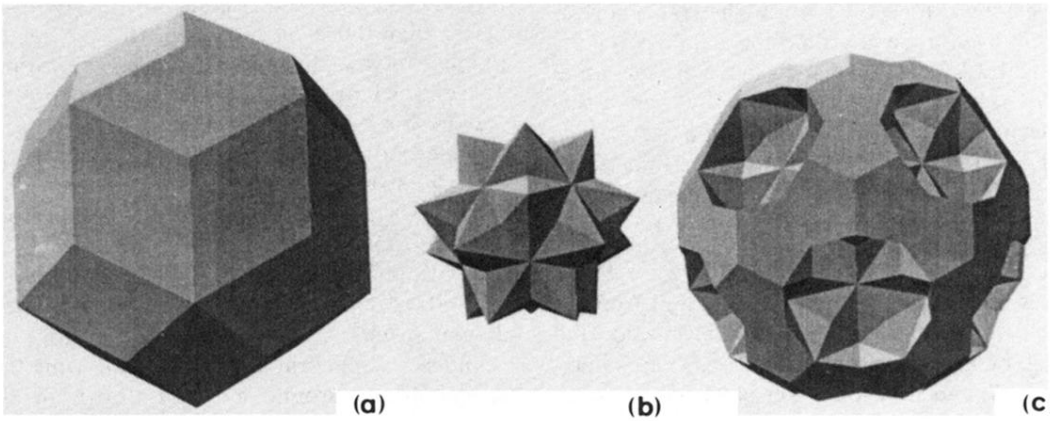

FIG. 7. Atomic surfaces of the model in perpendicular space: (a) P_{n_1} at node n_1 (triacontahedron), (b) P_{bc_1} at body center bc_1, and (c) P_{n_2} at node n_2 (triacontahedron truncated by P_{bc_1}).